Chapter 12

High-Frequency Techniques

Historically, given the limitations of computer power and memory, and in the absence of advanced algorithms such as the ACA, MLACA, or MLFMA, use of the MoM was limited to a full-matrix approach and problems of very small electrical size. As electrically large problems have always been of interest, alternative approaches and solution techniques are at times necessary to solve practical problems. In this chapter we describe several of these alterative approaches, which are referred to as "high-frequency" techniques. In general, these techniques make approximations to the surface integral equations of scattering (Section 3.6) in the high-frequency or asymptotic limit, making their solution far more tractable for electrically large targets. Though less accurate, they continue to be used due to their ease of use, speed and ability to produce data in situations where CPU or compute time is limited, making the use of MoM less attractive or even impossible. The techniques described herein are implemented in he commercially available Tripoint Industries high-frequency solver *lucernhammer MT*.

12.1 Physical Optics (PO)

Physical Optics (PO), discussed briefly in Section 6.1.1, is one of the oldest and most widely used high-frequency approximations, and it is the foundation of many of the techniques used herein. Consider now an electrically large object, whose size is (at least) ten electrical wavelengths in each dimension. In PO, it is assumed that at any point on this object, the surface can be considered locally planar and infinite in extent. Under this approximation, the scattered (or reflected) fields $\mathbf{E}^s(\mathbf{r})$ and $\mathbf{H}^s(\mathbf{r})$ at the surface are related directly to the incident fields $\mathbf{E}^i(\mathbf{r})$ and $\mathbf{H}^i(\mathbf{r})$ via simple planar reflection coefficients, which are known *a priori*. With all the fields known, the currents $\mathbf{M}(\mathbf{r})$ and $\mathbf{J}(\mathbf{r})$ are simply

$$\mathbf{M}(\mathbf{r}) = -\hat{\mathbf{n}} \times \left[\mathbf{E}^i(\mathbf{r}) + \mathbf{E}^s(\mathbf{r})\right] \tag{12.1}$$

and

$$\mathbf{J}(\mathbf{r}) = \hat{\mathbf{n}} \times \left[\mathbf{H}^i(\mathbf{r}) + \mathbf{H}^s(\mathbf{r})\right] \ , \tag{12.2}$$

where by the extinction theorem, the fields inside the object are assumed to be zero. The scattered far electric field is then obtained directly via (3.133). This yields what is called a "first bounce" scattered field, as it is due to the first "bounce" of the incident field. PO assumes that the currents exist only on surfaces that are directly illuminated by the incident field, and are zero in shadowed areas, which is not true in reality. Therefore, while PO can be reasonably accurate at near-specular angles, it often performs poorly elsewhere. Scattered fields due to "higher bounces", comprising multiple reflections on the target's surface, or penetration and transmission of the incident field across an exterior dielectric boundary into the interior of the object, are handled by the Shooting and Bouncing Ray (SBR) technique, discussed in Section 12.2.

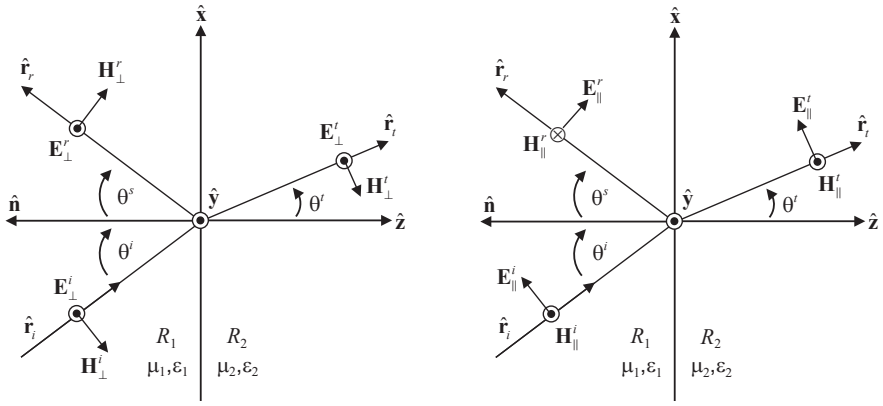
12.1.1 Plane Wave Decomposition At A Planar Interface

As already mentioned, the PO technique relates the scattered field at the (locally planar) surface of the object to the incident fields in terms of planar reflection coefficients. We first discuss the decomposition of incident, reflected, and transmitted fields at a planar dielectric interface. We then consider several other types of interfaces.

To begin, consider the geometry in Figure 12.1, where a plane wave traveling in the $\hat{\mathbf{z}}$ direction is incident on a dielectric boundary in the xy plane, where the incident region R_1 comprises $z < 0$, with dielectric parameters μ_1, ϵ_1, and $\eta_1 = \sqrt{\mu_1/\epsilon_1}$, and the transmitted region R_2 comprises $z > 0$, with dielectric parameters μ_2, ϵ_2, and $\eta_2 = \sqrt{\mu_2/\epsilon_2}$. At this boundary, the incident field $\mathbf{E}^i$ gives rise to the reflected field $\mathbf{E}^r$ in R_1 and the transmitted field $\mathbf{E}^t$ in R_2, respectively. The incident, reflected, and transmitted directions are, respectively,

$$\hat{\mathbf{r}}_i = \cos\theta_i \hat{\mathbf{z}} + \sin\theta_i \hat{\mathbf{x}} \,, \tag{12.3}$$

$$\hat{\mathbf{r}}_r = -\cos\theta_r \hat{\mathbf{z}} + \sin\theta_r \hat{\mathbf{x}} \,, \tag{12.4}$$



(a) Perpendicular (TM) Polarization

(b) Parallel (TE) Polarization

Figure 12.1: Plane Wave Incidence on Boundary: Perpendicular and Parallel Polarization

and

$$\hat{\mathbf{r}}_t = \cos\theta_t \hat{\mathbf{z}} + \sin\theta_t \hat{\mathbf{x}} \,, \tag{12.5}$$

with the Snell's law relationships $\theta_i = \theta_r$ and $k_1 \sin\theta_i = k_2 \sin\theta_t$, and the wavenumbers k_1 and k_2 may be complex. At the interface, the electric field can be decomposed into perpendicular ($\perp$) and parallel ($\parallel$) components $\mathbf{E}^i_\perp$ and $\mathbf{E}^i_\parallel$, as shown in Figures 12.1a and 12.1b, respectively.

12.1.1.1 Dielectric Boundary: Perpendicular Polarization

Assuming an incident electric field of unit amplitude, the incident, reflected, and transmitted electric fields $\mathbf{E}_r$, $\mathbf{E}_r$, and $\mathbf{E}_t$ for perpendicular polarization are

$$\mathbf{E}_i = \hat{\mathbf{y}} \,, \quad \mathbf{E}_r = \Gamma_\perp \hat{\mathbf{y}} \,, \quad \mathbf{E}_t = \mathrm{T}_\perp \hat{\mathbf{y}} \,, \tag{12.6}$$

where $\Gamma_\perp$ and $\mathrm{T}_\perp$ are the planar reflection and transmission coefficients for perpendicular polarization, respectively. The boundary conditions on the electric field require continuous tangential components across the boundary, and as the fields in (12.6) are already tangential, $\mathbf{E}_i + \mathbf{E}_r = \mathbf{E}_t$, and

$$1 + \Gamma_\perp = \mathrm{T}_\perp \,. \tag{12.7}$$

The corresponding incident, reflected, and transmitted magnetic fields $\mathbf{H}_r$, $\mathbf{H}_r$, and $\mathbf{H}_t$ are, respectively,

$$\mathbf{H}_i = \frac{1}{\eta_1} \hat{\mathbf{r}}_i \times \mathbf{E}_i = \frac{1}{\eta_1} (-\cos\theta_i \hat{\mathbf{x}} + \sin\theta_i \hat{\mathbf{z}}) \,, \tag{12.8}$$

$$\mathbf{H}_r = \frac{1}{\eta_1} \hat{\mathbf{r}}_r \times \mathbf{E}_r = \frac{\Gamma_\perp}{\eta_1} (\cos\theta_r \hat{\mathbf{x}} + \sin\theta_r \hat{\mathbf{z}}) \,, \tag{12.9}$$

and

$$\mathbf{H}_t = \frac{1}{\eta_2} \hat{\mathbf{r}}_t \times \mathbf{E}_t = \frac{\mathrm{T}_\perp}{\eta_2} (-\cos\theta_t \hat{\mathbf{x}} + \sin\theta_t \hat{\mathbf{z}}) \,. \tag{12.10}$$

As the reflection and transmission coefficients for a dielectric interface are already well known, we simply summarize them here. They are [1]

$$\Gamma_\perp = \frac{\eta_2 \cos\theta_i - \eta_1 \cos\theta_t}{\eta_2 \cos\theta_i + \eta_1 \cos\theta_t} \,, \tag{12.11}$$

and

$$\mathrm{T}_\perp = \frac{2\eta_2 \cos\theta_i}{\eta_2 \cos\theta_i + \eta_1 \cos\theta_t} \,. \tag{12.12}$$

12.1.1.2 Dielectric Boundary: Parallel Polarization

Assuming an incident electric field of unit amplitude, the incident, reflected, and transmitted electric fields $\mathbf{E}_r$, $\mathbf{E}_r$, and $\mathbf{E}_t$ for parallel polarization are

$$\mathbf{E}_i = \cos\theta_i \hat{\mathbf{x}} - \sin\theta_i \hat{\mathbf{z}} \,, \tag{12.13}$$

$$\mathbf{E}_r = \Gamma_\parallel(\cos\theta_r\hat{\mathbf{x}} + \sin\theta_r\hat{\mathbf{z}}) \,, \tag{12.14}$$

and

$$\mathbf{E}_t = \mathrm{T}_\parallel(\cos\theta_t\hat{\mathbf{x}} - \sin\theta_t\hat{\mathbf{z}}) \,. \tag{12.15}$$

where $\Gamma_\parallel$ and $\mathrm{T}_\parallel$ are the reflection and transmission coefficients for parallel polarization, respectively. Equating the tangential components of $\mathbf{E}$ on each side of the boundary then yields

$$\cos\theta_i + \Gamma_\parallel\cos\theta_r = \mathrm{T}_\parallel\cos\theta_t \,, \tag{12.16}$$

or

$$\Gamma_\parallel = \frac{\mathrm{T}_\parallel\cos\theta_t - \cos\theta_i}{\cos\theta_i} \,, \tag{12.17}$$

and

$$\mathrm{T}_\parallel = \frac{\cos\theta_i}{\cos\theta_t}(1 + \Gamma_\parallel) \,. \tag{12.18}$$

The corresponding incident, reflected, and transmitted magnetic fields $\mathbf{H}_r$, $\mathbf{H}_r$, and $\mathbf{H}_t$ are, respectively,

$$\mathbf{H}_i = \frac{1}{\eta_1}\hat{\mathbf{r}}_i \times \mathbf{E}_i = \frac{1}{\eta_1}\hat{\mathbf{y}} \,, \tag{12.19}$$

$$\mathbf{H}_r = \frac{1}{\eta_1}\hat{\mathbf{r}}_r \times \mathbf{E}_r = -\frac{\Gamma_\parallel}{\eta_1}\hat{\mathbf{y}} \,, \tag{12.20}$$

and

$$\mathbf{H}_t = \frac{1}{\eta_2}\hat{\mathbf{r}}_t \times \mathbf{E}_t = \frac{\mathrm{T}_\parallel}{\eta_2}\hat{\mathbf{y}} \,. \tag{12.21}$$

As the reflection and transmission coefficients for a dielectric interface are already well known, we simply summarize them here. They are [1]

$$\Gamma_\parallel = \frac{\eta_2\cos\theta_t - \eta_1\cos\theta_i}{\eta_2\cos\theta_t + \eta_1\cos\theta_i} \,, \tag{12.22}$$

and

$$\mathrm{T}_\parallel = \frac{2\eta_2\cos\theta_i}{\eta_2\cos\theta_t + \eta_1\cos\theta_i} \,. \tag{12.23}$$

12.1.1.3 Resistive Boundary: Perpendicular Polarization

We will first derive the coefficients for perpendicular polarization, as shown in Figure 12.1a. The tangential electric field is continuous across the boundary, and for the magnetic field, we enforce the boundary conditions in (3.227). We first compute

$$\hat{\mathbf{n}} \times \mathbf{H}_1 = -\hat{\mathbf{z}} \times (\mathbf{H}_i + \mathbf{H}_r) = \frac{1}{\eta_1}(\cos\theta_i - \Gamma_\perp\cos\theta_r)\hat{\mathbf{y}} \tag{12.24}$$

and

$$\hat{\mathbf{n}} \times \mathbf{H}_2 = -\hat{\mathbf{z}} \times \mathbf{H}_t = \frac{\mathrm{T}_\perp}{\eta_2}\cos\theta_t\hat{\mathbf{y}} \,. \tag{12.25}$$

Substitution of (12.6), (12.24) and (12.25) into (3.227) then yields

$$\frac{1}{2R}(1+\Gamma_\perp+\mathrm{T}_\perp)=\frac{1}{\eta_1}(\cos\theta_i-\Gamma_\perp\cos\theta_r)-\frac{\mathrm{T}_\perp}{\eta_2}\cos\theta_t\ , \tag{12.26}$$

where after using (12.7) and some straightforward but lengthy algebra, we obtain

$$\Gamma_\perp=\frac{\eta_2\cos\theta_i-\eta_1\cos\theta_t-\frac{\eta_1\eta_2}{R}}{\eta_2\cos\theta_i+\eta_1\cos\theta_t+\frac{\eta_1\eta_2}{R}}\ , \tag{12.27}$$

and

$$\mathrm{T}_\perp=\frac{2\eta_2\cos\theta_i}{\eta_2\cos\theta_i+\eta_1\cos\theta_t+\frac{\eta_1\eta_2}{R}}\ . \tag{12.28}$$

When $R\to 0$, the interface tends towards a perfect conductor, and $\Gamma_\perp=-1$ and $\mathrm{T}_\perp=0$, as expected. Similarly, when $R\to\infty$, the terms involving R vanish and $\Gamma_\perp$ and $\mathrm{T}_\perp$ become the regular reflection and transmission coefficients for a dielectric boundary.

12.1.1.4 Resistive Boundary: Parallel Polarization

We will next derive the coefficients for parallel polarization, as shown in Figure 12.1b. Equating the tangential components of the electric field on each side of the boundary from (12.13) – (12.15), we obtain

$$\cos\theta_i+\Gamma_\parallel\cos\theta_r=\mathrm{T}_\parallel\cos\theta_t\ , \tag{12.29}$$

or

$$\Gamma_\parallel=\frac{\mathrm{T}_\parallel\cos\theta_t-\cos\theta_i}{\cos\theta_i}\ , \tag{12.30}$$

and

$$\mathrm{T}_\parallel=\frac{\cos\theta_i}{\cos\theta_t}(1+\Gamma_\parallel)\ . \tag{12.31}$$

Following (3.227), we first compute for the electric fields

$$\hat{\mathbf{n}}\times\hat{\mathbf{n}}\times(\mathbf{E}_1+\mathbf{E}_2)=\hat{\mathbf{z}}\times\hat{\mathbf{z}}\times[\mathbf{E}_i+\mathbf{E}_r+\mathbf{E}_t]=-[\cos\theta_i+\Gamma_\parallel\cos\theta_r+\mathrm{T}_\parallel\cos\theta_t]\hat{\mathbf{x}}\,, \tag{12.32}$$

and for the magnetic fields,

$$\hat{\mathbf{n}}\times(\mathbf{H}_1-\mathbf{H}_2)=-\hat{\mathbf{z}}\times(\mathbf{H}_i+\mathbf{H}_r-\mathbf{H}_t)=\Big[\frac{1}{\eta_1}-\frac{\Gamma_\parallel}{\eta_1}-\frac{\mathrm{T}_\parallel}{\eta_2}\Big]\hat{\mathbf{x}}\,. \tag{12.33}$$

Then, following (3.227), we obtain

$$\frac{1}{2R}[\cos\theta_i+\Gamma_\parallel\cos\theta_r+\mathrm{T}_\parallel\cos\theta_t]=\Big[\frac{1}{\eta_1}-\frac{\Gamma_\parallel}{\eta_1}-\frac{\mathrm{T}_\parallel}{\eta_2}\Big]\ . \tag{12.34}$$

Substitution of (12.31) into the above, and performing some straightforward but lengthy algebra then yields

$$\Gamma_\parallel=\frac{\eta_2\cos\theta_t-\eta_1\cos\theta_i-\frac{\eta_1\eta_2}{R}\cos\theta_i\cos\theta_t}{\eta_2\cos\theta_t+\eta_1\cos\theta_i+\frac{\eta_1\eta_2}{R}\cos\theta_i\cos\theta_t}\ , \tag{12.35}$$

and using (12.31) in (12.35) yields

$$\mathrm{T}_{\parallel} = \frac{2\eta_2 \cos\theta_i}{\eta_2 \cos\theta_t + \eta_1 \cos\theta_i + \frac{\eta_1\eta_2}{R}\cos\theta_i \cos\theta_t} \,. \tag{12.36}$$

When $R \to 0$, the interface tends towards a perfect conductor, and $\Gamma_{\parallel} = -1$ and $\mathrm{T}_{\parallel} = 0$, as expected. Similarly, when $R \to \infty$, the terms involving R vanish and $\Gamma_{\parallel}$ and $\mathrm{T}_{\parallel}$ become the regular reflection and transmission coefficients for a dielectric boundary.

12.1.1.5 Reflection Coefficients for the Leontovich IBC

Given the equivalent impedance Z for the Lenotovich IBC, the effective reflection coefficient R for both polarizations is [2]

$$R = \frac{Z - \eta_l}{Z + \eta_l} \,, \tag{12.37}$$

where $\eta_l = \sqrt{\mu_l/\epsilon_l}$ is the intrinsic impedance of region R_l. As noted previously, while Z is frequency dependent, R in (12.37) assumes normal incidence and is therefore polarization independent.

12.1.1.6 Layered Dielectric Stack

In addition to interfaces between two homogeneous, bulk dielectric materials, many objects have thin coatings which comprise a stack-up of many thin dielectric layers. This is common with reentry vehicles or aircraft, where surfaces, often PEC-backed,

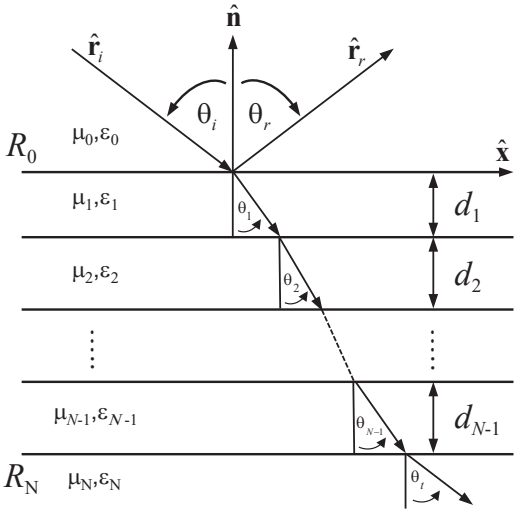


Figure 12.2: Layered Dielectric Stack

are coated with a thin layer of radar absorbing material (RAM). Such a multi-layer geometry is illustrated in Figure 12.2, comprising a stack of layers each having its own thickness d and dielectric parameters (μ, ϵ). In this case, we are interested in *effective* reflection coefficients $(R_\perp,\ R_\parallel)$ at the outermost interface in R_0, and likewise the *effective* transmission coefficients $(T_\perp, T_\parallel)$ into R_N, taking into account the reflections and transmissions between the layers.

The effective reflection and transmission coefficients can be determined using the recursion relationships [2]

$$R_i = \frac{r_{i,i+1} + R_{i+1} e^{-2jk_{i+1,z}d_{i+1}}}{1 + r_{i,i+1} R_{i+1} e^{-2jk_{i+1,z}d_{i+1}}} \,, \tag{12.38}$$

and

$$T_i = \frac{t_{i,i+1} T_{i+1} e^{-jk_{i+1,z}d_{i+1}}}{1 + r_{i,i+1} R_{i+1} e^{-2jk_{i+1,z}d_{i+1}}} \,, \tag{12.39}$$

At each step, R_i and T_i represent the *total* reflection and transmission coefficients, respectively, at the interface between layers i and $i+1$. The coefficients $r_{i,i+1}$ and $t_{i,i+1}$ are the *elementary* reflection and transmission coefficients, respectively, at the interface between layers i and $i+1$, summarized previously in (12.11) and (12.12), and (12.22) and (12.23), for perpendicular and arallel polarizations, respectively. The term $k_{i,z}$ comprises the $\hat{\mathbf{z}}$ component of the wavenumber in layer i, i.e.

$$k_{i,z} = k_i \cos\theta_i \,, \tag{12.40}$$

where following Snell's law,

$$\cos\theta_i = \sqrt{1 - k_0^2/k_i^2 \sin^2\theta_0} \,. \tag{12.41}$$

The recursions in (12.38) and (12.39) begin at the interface between layer $N-1$ and region R_N, and work backwards layer by layer until we reach the interface between region R_0 and layer 1. If R_N comprises PEC, $r_{N-1,N} = -1$, and there is no transmission through the stack.

12.1.2 Field Scattered At An Interface

To compute the field scattered at an interface, we must determine expressions for the currents **J** and **M** on the interface. As in practice we will be working on flat, planar triangles at arbitrary orientations, it makes sense to define a local coordinate system to work in, as shown in Figure 12.3. At each location, given a surface normal $\hat{\mathbf{n}}$, we can define a local right-handed coordinate system similar to that of Figure 12.1, with basis vectors given by

$$\hat{\mathbf{b}} = \frac{\hat{\mathbf{r}}_i \times \hat{\mathbf{n}}}{|\hat{\mathbf{r}}_i \times \hat{\mathbf{n}}|} \tag{12.42}$$

and

$$\hat{\mathbf{t}} = \hat{\mathbf{n}} \times \hat{\mathbf{b}} \,, \tag{12.43}$$

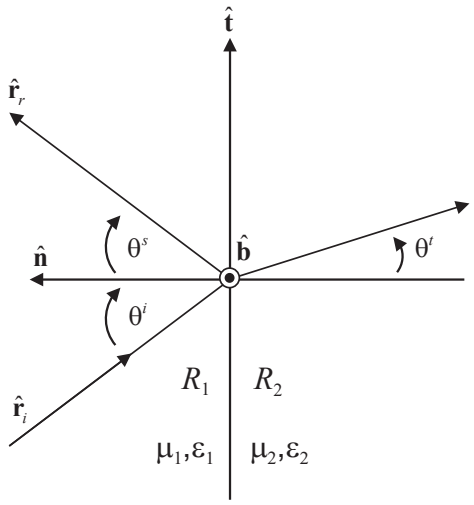


Figure 12.3: Local Interface Coordinate System

Substituting the total incident and reflected electric and magnetic fields from R_1 into (12.1) and (12.2) yields

$$\mathbf{M} = -\hat{\mathbf{n}} \times \left[(\mathbf{E}^i_\perp + \mathbf{E}^r_\perp) + (\mathbf{E}^i_\parallel + \mathbf{E}^r_\parallel) \right] \tag{12.44}$$

and

$$\mathbf{J} = \hat{\mathbf{n}} \times \left[(\mathbf{H}^i_\perp + \mathbf{H}^r_\perp) + (\mathbf{H}^i_\parallel + \mathbf{H}^r_\parallel) \right] . \tag{12.45}$$

As **M** and **J** have no components along $\hat{\mathbf{n}}$, we can rewrite the above as

$$\mathbf{M} = -\hat{\mathbf{n}} \times \left[E_b \hat{\mathbf{b}} + E_t \hat{\mathbf{t}} \right] \tag{12.46}$$

and

$$\mathbf{J} = \hat{\mathbf{n}} \times \left[H_b \hat{\mathbf{b}} + H_t \hat{\mathbf{t}} \right] , \tag{12.47}$$

where

$$E_b = \mathbf{E}^i \cdot \hat{\mathbf{b}} \left(1 + R_\perp \right) , \tag{12.48}$$

$$E_t = \mathbf{E}^i \cdot \hat{\mathbf{t}} \left(1 + R_\parallel \right) , \tag{12.49}$$

$$H_b = \mathbf{H}^i \cdot \hat{\mathbf{b}} \left(1 - R_\parallel \right) , \tag{12.50}$$

$$H_t = \mathbf{H}^i \cdot \hat{\mathbf{t}} \left(1 - R_\perp \right) . \tag{12.51}$$

Substitution of (12.48) and (12.49) into (12.44) and (12.50) and (12.51) into (12.45) then allows us to write

$$\mathbf{M} = \mathbf{E}^i \cdot \overline{\mathbf{R}}_e \times \hat{\mathbf{n}} , \tag{12.52}$$

and

$$\mathbf{J} = -\mathbf{H}^i \cdot \overline{\mathbf{R}}_h \times \hat{\mathbf{n}} , \tag{12.53}$$

where the dyadics $\overline{\mathbf{R}}_e$ and $\overline{\mathbf{R}}_h$ are

$$\overline{\mathbf{R}}_e = (1 + R_\perp)\hat{\mathbf{b}}\hat{\mathbf{b}} + (1 + R_\parallel)\hat{\mathbf{t}}\hat{\mathbf{t}} \tag{12.54}$$

and

$$\overline{\mathbf{R}}_h = (1 - R_\parallel)\hat{\mathbf{b}}\hat{\mathbf{b}} + (1 - R_\perp)\hat{\mathbf{t}}\hat{\mathbf{t}}\,. \tag{12.55}$$

Using the relationships between $\hat{\mathbf{n}}$, $\hat{\mathbf{b}}$, and $\hat{\mathbf{t}}$, we can then rewrite (12.52) and (12.53) as

$$\mathbf{M} = \mathbf{E}^i \cdot \overline{\mathbf{R}}_e'\,, \tag{12.56}$$

and

$$\mathbf{J} = \mathbf{H}^i \cdot \overline{\mathbf{R}}_h'\,, \tag{12.57}$$

where

$$\overline{\mathbf{R}}_e' = -(1 + R_\perp)\hat{\mathbf{b}}\hat{\mathbf{t}} + (1 + R_\parallel)\hat{\mathbf{t}}\hat{\mathbf{b}} \tag{12.58}$$

and

$$\overline{\mathbf{R}}_h' = (1 - R_\parallel)\hat{\mathbf{b}}\hat{\mathbf{t}} - (1 - R_\perp)\hat{\mathbf{t}}\hat{\mathbf{b}}\,. \tag{12.59}$$

Using (3.133), we can then write a generalized expression for the total scattered electric far field $\mathbf{E}^s(\mathbf{r})$ in the exterior region R_0 as

$$\mathbf{E}^s(\mathbf{r}) = -\frac{j\omega e^{-jk_0 r}}{4\pi r}\Big(\big[A_\theta(\mathbf{r}) + \eta_0 F_\phi(\mathbf{r})\big]\hat{\boldsymbol{\theta}}^s + \big[A_\phi(\mathbf{r}) - \eta_0 F_\theta(\mathbf{r})\big]\hat{\boldsymbol{\phi}}^s\Big)\,, \tag{12.60}$$

where

$$A_\theta = \mathbf{A}\cdot\hat{\boldsymbol{\theta}}^s, \quad A_\phi = \mathbf{A}\cdot\hat{\boldsymbol{\phi}}^s, \quad F_\theta = \mathbf{F}\cdot\hat{\boldsymbol{\theta}}^s, \quad F_\phi = \mathbf{F}\cdot\hat{\boldsymbol{\phi}}^s\,, \tag{12.61}$$

and

$$\mathbf{A}(\mathbf{r}) = \mu_0 \int \mathbf{H}^i(\mathbf{r}')\cdot\overline{\mathbf{R}}_h'\, e^{jk_0\hat{\mathbf{r}}^s\cdot\mathbf{r}'}\, d\mathbf{r}' \tag{12.62}$$

and

$$\mathbf{F}(\mathbf{r}) = \epsilon_0 \int \mathbf{E}^i(\mathbf{r}')\cdot\overline{\mathbf{R}}_e'\, e^{jk_0\hat{\mathbf{r}}^s\cdot\mathbf{r}'}\, d\mathbf{r}'\,. \tag{12.63}$$

These expressions can be further simplified to create a scattering matrix for first-bounce scattering.

12.1.2.0.1 First-Bounce Scattered Field At An Interface

Given the incident $\hat{\boldsymbol{\theta}}^i$- and $\hat{\boldsymbol{\phi}}^i$-polarized incident electric and magnetic fields in (3.137) and (3.138), we can then write (12.56) and (12.57) for $\hat{\boldsymbol{\theta}}^i$-incidence as

$$\mathbf{M}(\mathbf{r}') = \hat{\boldsymbol{\theta}}^i\cdot\overline{\mathbf{R}}_e' e^{jk_0\hat{\mathbf{r}}^i\cdot\mathbf{r}'}, \quad \mathbf{J}(\mathbf{r}') = -\frac{1}{\eta_0}\hat{\boldsymbol{\phi}}^i\cdot\overline{\mathbf{R}}_h' e^{jk_0\hat{\mathbf{r}}^i\cdot\mathbf{r}'}, \tag{12.64}$$

and for $\hat{\boldsymbol{\phi}}^i$-incidence as

$$\mathbf{M}(\mathbf{r}') = \hat{\boldsymbol{\phi}}^i\cdot\overline{\mathbf{R}}_e' e^{jk_0\hat{\mathbf{r}}^i\cdot\mathbf{r}'}, \quad \mathbf{J}(\mathbf{r}') = \frac{1}{\eta_0}\hat{\boldsymbol{\theta}}^i\cdot\overline{\mathbf{R}}_h' e^{jk_0\hat{\mathbf{r}}^i\cdot\mathbf{r}'}. \tag{12.65}$$

where the incident electric field has unit amplitude. The elements of the corresponding scattering matrix (3.139) can then be obtained via (12.60), and are

$$S_{\theta\theta} = \big[-\hat{\boldsymbol{\phi}}^{\,i} \cdot \overline{\mathbf{R}}'_h \cdot \hat{\boldsymbol{\theta}}^{\,s} + \hat{\boldsymbol{\theta}}^{\,i} \cdot \overline{\mathbf{R}}'_e \cdot \hat{\boldsymbol{\phi}}^{\,s} \big] \mathrm{I}_{po} \,, \tag{12.66}$$

$$S_{\phi\theta} = \big[-\hat{\boldsymbol{\phi}}^{\,i} \cdot \overline{\mathbf{R}}'_h \cdot \hat{\boldsymbol{\phi}}^{\,s} - \hat{\boldsymbol{\theta}}^{\,i} \cdot \overline{\mathbf{R}}'_e \cdot \hat{\boldsymbol{\theta}}^{\,s} \big] \mathrm{I}_{po} \,, \tag{12.67}$$

$$S_{\theta\phi} = \big[\hat{\boldsymbol{\theta}}^{\,i} \cdot \overline{\mathbf{R}}'_h \cdot \hat{\boldsymbol{\theta}}^{\,s} + \hat{\boldsymbol{\phi}}^{\,i} \cdot \overline{\mathbf{R}}'_e \cdot \hat{\boldsymbol{\phi}}^{\,s} \big] \mathrm{I}_{po} \,, \tag{12.68}$$

and

$$S_{\phi\phi} = \big[\hat{\boldsymbol{\theta}}^{\,i} \cdot \overline{\mathbf{R}}'_h \cdot \hat{\boldsymbol{\phi}}^{\,s} - \hat{\boldsymbol{\phi}}^{\,i} \cdot \overline{\mathbf{R}}'_e \cdot \hat{\boldsymbol{\theta}}^{\,s} \big] \mathrm{I}_{po} \,, \tag{12.69}$$

where

$$\mathrm{I}_{po} = -\frac{j}{2\lambda_0} \int e^{jk_0(\hat{\mathbf{r}}^i + \hat{\mathbf{r}}^s)\cdot \mathbf{r}'} \, d\mathbf{r}' \,, \tag{12.70}$$

and the $e^{-jk_0 r}/r$ term has been omitted. When the phase integral in (12.70) is evaluated over a particular shape, it is referred to as a *shape function*. This integral is evaluated analytically over a planar triangle in Section 13.2.2.

12.1.2.1 First-Bounce Scattered Field At A PEC Interface

If the object is PEC, then $\mathrm{R}_\perp = \mathrm{R}_\parallel = -1$, $\mathbf{M}(\mathbf{r}) = 0$, and the tangential reflected magnetic field is equal in amplitude and phase to the tangential incident magnetic field at the surface. The electric surface current can then be written as

$$\mathbf{J}(\mathbf{r}) = 2\hat{\mathbf{n}} \times \mathbf{H}^i(\mathbf{r}) \,, \tag{12.71}$$

and the elements of the scattering matrix are then

$$S_{\theta\theta} = -2\big[\hat{\mathbf{n}} \times \hat{\boldsymbol{\phi}}^{\,i}\big] \cdot \hat{\boldsymbol{\theta}}^{\,s} \, \mathrm{I}_{po} = 2\hat{\mathbf{n}} \cdot \big[\hat{\boldsymbol{\theta}}^{\,s} \times \hat{\boldsymbol{\phi}}^{\,i}\big] \, \mathrm{I}_{po} \,, \tag{12.72}$$

$$S_{\phi\theta} = -2\big[\hat{\mathbf{n}} \times \hat{\boldsymbol{\phi}}^{\,i}\big] \cdot \hat{\boldsymbol{\phi}}^{\,s} \, \mathrm{I}_{po} = 2\hat{\mathbf{n}} \cdot \big[\hat{\boldsymbol{\phi}}^{\,s} \times \hat{\boldsymbol{\phi}}^{\,i}\big] \, \mathrm{I}_{po} \,, \tag{12.73}$$

$$S_{\theta\phi} = 2\big[\hat{\mathbf{n}} \times \hat{\boldsymbol{\theta}}^{\,i}\big] \cdot \hat{\boldsymbol{\theta}}^{\,s} \, \mathrm{I}_{po} = 2\hat{\mathbf{n}} \cdot \big[\hat{\boldsymbol{\theta}}^{\,i} \times \hat{\boldsymbol{\theta}}^{\,s}\big] \, \mathrm{I}_{po} \,, \tag{12.74}$$

and

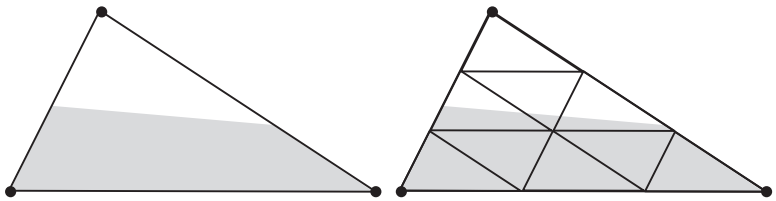
$$S_{\phi\phi} = 2\big[\hat{\mathbf{n}} \times \hat{\boldsymbol{\theta}}^{\,i}\big] \cdot \hat{\boldsymbol{\phi}}^{\,s} \, \mathrm{I}_{po} = 2\hat{\mathbf{n}} \cdot \big[\hat{\boldsymbol{\theta}}^{\,i} \times \hat{\boldsymbol{\phi}}^{\,s}\big] \, \mathrm{I}_{po} \,. \tag{12.75}$$

where I_{po} is defined in (12.70). It is worth noting that for monostatic scattering, $\hat{\boldsymbol{\theta}}^{\,s} = \hat{\boldsymbol{\theta}}^{\,i}$ and $\hat{\boldsymbol{\phi}}^{\,s} = \hat{\boldsymbol{\phi}}^{\,i}$, therefore

$$S_{\theta\theta} = S_{\phi\phi} \tag{12.76}$$

and

$$S_{\phi\theta} = S_{\theta\phi} = 0 \,. \tag{12.77}$$



(a) Original Triangle (b) Subdivided Triangle

Figure 12.4: Partially Illuminated Triangle

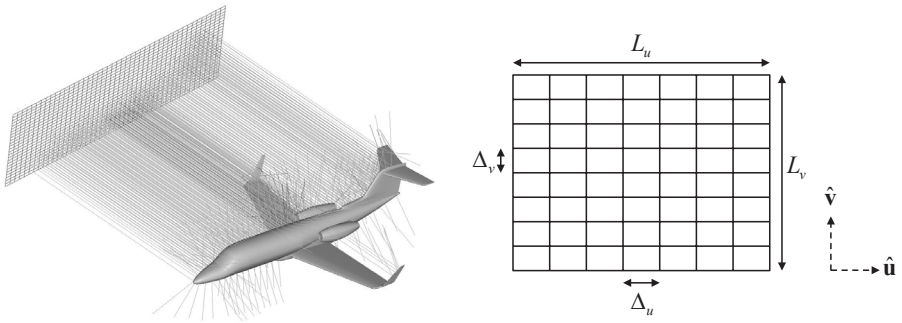
12.1.2.2 Illumination and Shadowing

PO assumes that the surface currents exist only on those portions of the surface that are directly illuminated by the incident field, and are zero elsewhere. Therefore, we must determine which triangles are illuminated or in shadow, which we do using a high-speed triangle ray tracer. For convex single objects, such as cones or frustums, each triangle is fully illuminated or shadowed. In this case, it is sufficient to cast a single shadow ray for each triangle. Concave objects or scenes with multiple targets self-shadow themselves from certain illumination angles, and some triangles may be partially illuminated, s shown in Figure 12.4a.

If a triangle is partially illuminated, the shape function (12.70) is no longer valid. This issue can be mitigated by subdividing the triangle into a number of smaller triangles, as shown in Figure 12.4b, where the sub-triangles have the same proportions as the parent triangle. The shadowing check is then done for each sub-triangle, and the scattered fields of illuminated sub-triangles then comprise a phase-shifted version of the others.

12.2 Shooting and Bouncing Rays (SBR)

Realistic objects, such as air and space vehicles, have fins, appendages and engine inlets which are significant contributors to the total scattering due to multiple reflections (multibounce) of the incident field. The effects on the scattered field typically comprise a significantly higher RCS at certain scattering angles, as well as returns which delayed in time. We treat these multibounce effects using the Shooting and Bouncing Ray (SBR) method, where the incident wave is treated as a bundle of many small, independent ray tubes. Each ray tube is "fired" at the target and its path traced according to Geometrical Optics (GO) theory as it bounces on the target, encountering fins, cavities, and other features, as shown in Figure 12.5a. At each bounce point, the incident fields are decomposed following Section 12.1.1, the correct reflection and/or transmission coefficients are applied, and a PO-type integral is performed over the projection of each ray tube on the target's surface (the aperture) in the exterior region. This technique was first applied in the calculation of backscattering from arbitrarily shaped cavities and waveguides [3, 4], and also for penetrable, inhomogeneous objects [5].



(a) Rays Fired at a Target (b) Shoot Window Definition

Figure 12.5: SBR and Shoot Window

12.2.1 Shoot Window

To represent the portion of the incident plane wave that is incidence on the target, we introduce the shoot window, a rectangular aperture in space from which the rays are fired, as shown in Figure 12.5b. For each incident vector $\hat{\mathbf{r}}^i$, a rectangle is constructed outside of the target's bounding box, forming a virtual camera with an othographic projection, as in computer graphics. The window's basis vectors in the u and v dimensions are given by

$$\hat{\mathbf{u}} = \hat{\boldsymbol{\phi}}^i \,, \tag{12.78}$$

and

$$\hat{\mathbf{v}} = -\hat{\boldsymbol{\theta}}^i \,. \tag{12.79}$$

Assuming the target's bounding box to have dimensions L_x, L_y, and L_z, the window dimensions L_u and L_v in screen space are

$$L_u = |L_y \cos\phi^i| + |L_x \sin\phi^i| \,, \tag{12.80}$$

and

$$L_v = |L_x \cos\phi^i \cos\theta^i| + |L_y \sin\phi^i \cos\theta^i| + |L_z \sin\theta^i| \,. \tag{12.81}$$

This guarantees that the two-dimensional projection of the target is completely enclosed by the window, and that no extraneous rays are fired. The window is subdivided in the $\hat{\mathbf{u}}$ and $\hat{\mathbf{v}}$ directions into a number of rectangular pixels, representing the ray tubes that are fired, each having a width and height of Δ_u and Δ_v, respectively. In SBR, at least 10 rays per wavelength in each direction is needed [3], with modern implementations using much denser grids (20 to 30 rays per wavelength).

12.2.2 SBR Scattered Field At An Interface

We now derive expressions for the SBR scattered field at an interface. Consider a ray tube incident on an object, where at the first bounce point $\mathbf{r}_1$, the phase ψ_1 of the incident fields is

$$\psi_1 = e^{jk_0 \hat{\mathbf{r}}^i \cdot \mathbf{r}_1} \,. \tag{12.82}$$

The phase ψ_n at a later bounce point $\mathbf{r}_n$ is then the sum of this initial phase plus the phase accumulated between bounces. This can be written as

$$\psi_n = \psi_1 \prod_{m=2}^{n} e^{jk_m|\mathbf{r}_m - \mathbf{r}_{m-1}|} \tag{12.83}$$

where k_m is the wavenumber of the dielectric region the ray traveled through between points $\mathbf{r}_{m-1}$ and $\mathbf{r}_m$. Then, at $\mathbf{r}_n$, an intersection is made between the ray tube and the locally planar surface, creating a projected footprint, or aperture, on the surface. The phase of the fields across the aperture can then be written as

$$\psi_t(\mathbf{r}) = \psi_n e^{-jk_0\hat{\mathbf{s}}\cdot(\mathbf{r}-\mathbf{r}_n)} \tag{12.84}$$

where $\hat{\mathbf{s}}$ is the exit direction of the ray at $\mathbf{r}_n$, which comprises either the reflected direction, upon reflection, or the transmitted direction, upon transmission. We note that in (12.84), $\psi_t(\mathbf{r})$ has a linear phase variation, and we have used k_0 as integrations for the scattered field are done only in the exterior region R_0.

At each bounce point, the incident electric field is decomposed and reflected (or transmitted) following Section 12.1.1. This yields a total aperture electric field given by

$$\mathbf{E}(\mathbf{r}) = \mathbf{E}_i(\mathbf{r}) + \mathbf{E}_r(\mathbf{r}) \tag{12.85}$$

if reflected, and

$$\mathbf{E}(\mathbf{r}) = \mathbf{E}_t(\mathbf{r}) \tag{12.86}$$

if transmitted. The corresponding total magnetic fields are, respectively,

$$\mathbf{H}(\mathbf{r}) = \frac{1}{\eta_0}\left[\hat{\mathbf{r}}_i \times \mathbf{E}_i(\mathbf{r}) + \hat{\mathbf{r}}_s \times \mathbf{E}_r(\mathbf{r})\right] , \tag{12.87}$$

and

$$\mathbf{H}(\mathbf{r}) = \frac{1}{\eta_0}\hat{\mathbf{r}}_t \times \mathbf{E}_t(\mathbf{r}) , \tag{12.88}$$

where $\hat{\mathbf{r}}_i$, $\hat{\mathbf{r}}_s$, and $\hat{\mathbf{r}}_t$ are the incident, reflected, and transmitted ray directions at $\mathbf{r}_n$. The corresponding surface currents are then given by (3.6) and (3.5).

$$\mathbf{M}(\mathbf{r}) = -\hat{\mathbf{n}} \times \mathbf{E}(\mathbf{r}) , \tag{12.89}$$

and

$$\mathbf{J}(\mathbf{r}) = \hat{\mathbf{n}} \times \mathbf{H}(\mathbf{r}) , \tag{12.90}$$

where $\hat{\mathbf{n}}$ is the surface normal at $\mathbf{r}_n$.

Using (12.60)–(12.63), we can now write expressions for the PO-type field scattered by the aperture. The elements of the scattering matrix are then

$$S_{\theta\theta} = \left[\mathbf{J}_\theta \cdot \hat{\boldsymbol{\theta}}^s + \mathbf{M}_\theta \cdot \hat{\boldsymbol{\phi}}^s\right] \mathrm{I}_{sbr} , \tag{12.91}$$

$$S_{\phi\theta} = \left[\mathbf{J}_\theta \cdot \hat{\boldsymbol{\phi}}^s + \mathbf{M}_\theta \cdot \hat{\boldsymbol{\theta}}^s\right] \mathrm{I}_{sbr} , \tag{12.92}$$

$$S_{\theta\phi} = \left[\mathbf{J}_\phi \cdot \hat{\boldsymbol{\theta}}^s + \mathbf{M}_\phi \cdot \hat{\boldsymbol{\phi}}^s\right] \mathrm{I}_{sbr} \ , \tag{12.93}$$

and

$$S_{\phi\phi} = \left[\mathbf{J}_\phi \cdot \hat{\boldsymbol{\phi}}^s + \mathbf{M}_\phi \cdot \hat{\boldsymbol{\theta}}^s\right] \mathrm{I}_{sbr} \ , \tag{12.94}$$

where $\mathbf{J}_\theta$ and $\mathbf{M}_\theta$ are due to the $\hat{\boldsymbol{\theta}}^i$-polarized incident electric field, and $\mathbf{J}_\phi$ and $\mathbf{M}_\phi$ are due to the $\hat{\boldsymbol{\phi}}^i$-polarized incident electric field, and we have again taken advantage of the fact that $\mathbf{J}$ is derived from $\mathbf{H}$, which is obtained from $\mathbf{E}$ at each bounce point with a $1/\eta$ scale factor. The phase integral is

$$\mathrm{I}_{sbr} = -\frac{j}{2\lambda_0}\psi_t \int e^{jk_0(\hat{\mathbf{s}}\cdot(\hat{\mathbf{r}}'-\mathbf{r}_n)+\hat{\mathbf{r}}^s\cdot\mathbf{r}')} \, d\mathbf{r}' \ . \tag{12.95}$$

To evaluate (12.95), we modify the integrand so that the aperture is centered at the origin. To do so, we note that $\mathbf{r}'$ can be written as $\mathbf{r}' = \mathbf{r}_n + \mathbf{a}'$, where $\mathbf{a}'$ is measured from the center of the aperture. Making this substitution allows us to then write

$$\mathrm{I}_{sbr} = -\frac{j}{2\lambda_0}\psi_t e^{jk_0\hat{\mathbf{r}}^s\cdot\mathbf{r}_n} \int e^{jk_0(\hat{\mathbf{r}}^s-\hat{\mathbf{s}})\cdot\mathbf{a}'} \, d\mathbf{a}' \ . \tag{12.96}$$

12.2.3 SBR Aperture Shape Function

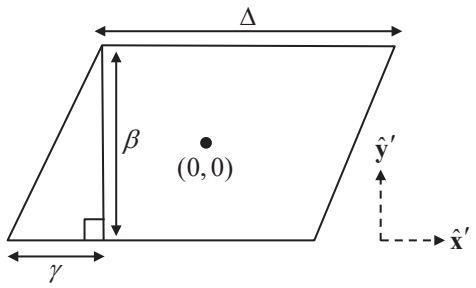


Figure 12.6: Projected Ray Tube Aperture

The intersection of a rectangular ray tube with a planar surface is a parallelogram, shown centered at the origin in Figure 12.6, where the base and height are Δ and β, respectively. To evaluate the phase integral in (12.96), we first define the vector

$$\mathbf{d} = k_0(\hat{\mathbf{r}}_s - \hat{\mathbf{s}}) \tag{12.97}$$

and

$$u = \mathbf{d}\cdot\hat{\mathbf{x}}' \ , \quad v = \mathbf{d}\cdot\hat{\mathbf{y}}' \ . \tag{12.98}$$

Doing so, the phase integral can now be written as

$$I = \int e^{jk_0(\hat{\mathbf{r}}^s-\hat{\mathbf{s}})\cdot\mathbf{a}'} \, d\mathbf{a}' = \int_A e^{j(ux'+vy')} \, dx' \, dy' \ . \tag{12.99}$$

where A is the aperture. Over the parallelogram, it can be written as

$$I = \int_{-\beta/2}^{\beta/2} e^{jvy'} \int_{\frac{\gamma}{\beta}y'-\Delta/2}^{\frac{\gamma}{\beta}y'+\Delta/2} e^{jux'}\, dx'\, dy' \,. \tag{12.100}$$

Evaluating the innermost integral yields

$$I = \frac{\Delta}{2}\text{sinc}\left[\frac{u\Delta}{2}\right] \int_{-\beta/2}^{\beta/2} e^{jy'\left(v+\frac{\gamma}{\beta}u\right)} dy' \,, \tag{12.101}$$

and evaluating the above yields the result

$$I = \int e^{jk_0\cdot(\hat{\mathbf{r}}^s-\hat{\mathbf{s}})\cdot\mathbf{a}'}\, d\mathbf{a}' = \beta\Delta\text{sinc}\left[\frac{u\gamma+v\beta}{2}\right]\text{sinc}\left[\frac{u\Delta}{2}\right] \,. \tag{12.102}$$

12.2.3.1 SBR Aperture Shape Function: Alternative Approach

We note that the phase integral in (12.99) has the form of a fourier transform. For an N-sided polygon of arbitrary shape, this integral can be evaluated analytically. If (x_n, y_n) comprise the coordinates of the polygon vertices, in clockwise order, the integral can be evaluated via the sum [6]

$$\int e^{j(ux'+vy')}\, dx'\, dy' = \sum_{n=1}^{N} e^{j(ux_n+vy_n)} \frac{p_{n-1}-p_n}{(u+p_{n-1}v)(u+p_nv)} \,, \tag{12.103}$$

where

$$p_n = \frac{y_{n+1}-y_n}{x_{n+1}-x_n} \,. \tag{12.104}$$

For the parallelogram in Figure 12.6, the vertices are clockwise from the lower left

$$(x_1, y_1) = \left(-\frac{\Delta+\gamma}{2}, -\frac{\beta}{2}\right) \,, \tag{12.105}$$

$$(x_2, y_2) = \left(-\frac{\Delta-\gamma}{2}, \frac{\beta}{2}\right) \,, \tag{12.106}$$

$$(x_3, y_3) = \left(\frac{\Delta+\gamma}{2}, \frac{\beta}{2}\right) \,, \tag{12.107}$$

$$(x_4, y_4) = \left(\frac{\Delta-\gamma}{2}, -\frac{\beta}{2}\right) \,. \tag{12.108}$$

Evaluating the sum (12.103) over the vertices then yields

$$\begin{aligned} I = &-\frac{\beta}{u}e^{j\left(-\frac{u}{2}(\Delta+\gamma)-v\frac{\beta}{2}\right)}\left[\frac{1}{u\gamma+v\beta}\right] + \frac{\beta}{u}e^{j\left(-\frac{u}{2}(\Delta+\gamma)+v\frac{\beta}{2}\right)}\left[\frac{1}{u\gamma+v\beta}\right] \\ &-\frac{\beta}{u}e^{j\left(\frac{u}{2}(\Delta+\gamma)+v\frac{\beta}{2}\right)}\left[\frac{1}{u\gamma+v\beta}\right] + \frac{\beta}{u}e^{j\left(\frac{u}{2}(\Delta-\gamma)-v\frac{\beta}{2}\right)}\left[\frac{1}{u\gamma+v\beta}\right] \,. \end{aligned} \tag{12.109}$$

or

$$I = \frac{\beta}{u} e^{-j\frac{u\Delta}{2}} \left[e^{\frac{j}{2}(u\gamma+v\beta)} - e^{-\frac{j}{2}(u\gamma+v\beta)} \right] - \frac{\beta}{u} e^{j\frac{u\Delta}{2}} \left[e^{\frac{j}{2}(u\gamma+v\beta)} - e^{-\frac{j}{2}(u\gamma+v\beta)} \right] . \tag{12.110}$$

Simplifying further yields

$$I = j\frac{\beta}{u} \text{sinc} \left[\frac{u\gamma + v\beta}{2} \right] \left[e^{-j\frac{u\Delta}{2}} - e^{j\frac{u\Delta}{2}} \right] \tag{12.111}$$

and finally,

$$I = \beta\Delta \text{sinc} \left[\frac{u\gamma + v\beta}{2} \right] \text{sinc} \left[\frac{u\Delta}{2} \right] , \tag{12.112}$$

which is the result in (12.102). Though the second approach was more laborious to evaluate in this case, it can be applied to polygons of arbitrary shape, whereas (12.100) was simpler but valid only for the parallelogram in Figure 12.6.

References

[1] C. A. Balanis, *Advanced Engineering Electromagnetics*. John Wiley and Sons, 1989.

[2] S. J. Orfanidis, "Electromagnetic waves and antennas." Electronic version: ece.rutgers.edu/ orfanidi/ewa/.

[3] H. Ling, S. W. Lee, and R. Chou, "Shooting and bouncing rays: calculating the RCS of an arbitrarily shaped cavity," *IEEE Trans. Antennas Propagat.*, vol. 37, pp. 194–205, February 1989.

[4] H. Ling, S. W. Lee, and R. Chou, "High-frequency RCS of open cavities with rectangular and circular cross sections," *IEEE Trans. Antennas Propagat.*, vol. 37, pp. 648–652, May 1989.

[5] H. Kim and H. Ling, "Electromagnetic scattering from an inhomogeneous object by ray tracing," *IEEE Trans. Antennas Propagat.*, vol. 40, pp. 517–525, May 1992.

[6] S. Lee and R. Mittra, "Fourier transform of a polygonal shape function and its application in electromagnetics," *IEEE Trans. Antennas Propagat.*, vol. 31, pp. 99–103, January 1983.